Significant Efficiency Enhancement of Hybrid Solar Cells Using Core–Shell Nanowire Geometry for Energy Harvesting

Shin-Hung Tsai,[†] Hung-Chih Chang,[†] Hsin-Hua Wang,[†] Szu-Ying Chen,[‡] Chin-An Lin,[†] Show-An Chen,[§] Yu-Lun Chueh,[‡] and Jr-Hau He[†,⊥,*]

[†]Institute of Photonics and Optoelectronics, National Taiwan University, Taipei, Taiwan, [‡]Department of Materials Science and Engineering, National Tsing Hua University, Hsinchu, Taiwan, [§]Department of Chemical Engineering, National Tsing Hua University, Hsinchu, Taiwan, and [⊥]Department of Electrical Engineering, National Taiwan University, Taipei, Taiwan

ABSTRACT A novel strategy employing core–shell nanowire arrays (NWAs) consisting of Si/regioregular poly-(3-hexylthiophene) (P3HT) was demonstrated to facilitate efficient light harvesting and exciton dissociation/charge collection for hybrid solar cells (HSCs). We experimentally demonstrate broadband and omnidirectional light-harvesting characteristics of core–shell NWA HSCs due to their subwavelength features, further supported by the simulation based on finite-difference time domain analysis. Meanwhile, core–shell geometry of NWA HSCs guarantees efficient charge separation since the thickness of the P3HT shells is comparable to the exciton diffusion length. Consequently, core–shell HSCs exhibit a 61% improvement of short-circuit current for a conversion efficiency (η) enhancement of 31.1% as compared to the P3HT-infiltrated Si NWA HSCs with layers forming a flat air/polymer cell interface. The improvement of crystal quality of P3HT shells due to the formation of ordering structure at Si interfaces after air mass 1.5 global (AM 1.5G) illumination was confirmed by transmission electron microscopy and Raman spectroscopy. The core–shell geometry with the interfacial improvement by AM 1.5G illumination promotes more efficient exciton dissociation and charge separation, leading to η improvement (~140.6%) due to the considerable increase in V_{oc} from 257 to 346 mV, J_{sc} from 11.7 to 18.9 mA/cm^2, and FF from 32.2 to 35.2%, which is not observed in conventional P3HT-infiltrated Si NWA HSCs. The stability of the Si/P3HT core–shell NWA HSCs in air ambient was carefully examined. The core–shell geometry should be applicable to many other material systems of solar cells and thus holds high potential in third-generation solar cells.

KEYWORDS: hybrid solar cells · core–shell · light harvesting · energy harvesting · nanowire

Organic photovoltaics (PVs) have received intensive attention due to their promising features, such as low cost, light weight, low-temperature process, and large-area production.[1] To improve the power conversion efficiency (η) of the pure organic PVs, an alternative is the class of organic–inorganic hybrid solar cells (HSCs), where the heterojunction with a large interfacial area is formed between organic polymers and inorganic semiconductors, facilitating fast electron transport with strong complementary absorption of organic semiconductors.[2−6] Due to very small diffusion length of the excitons (<15 nm), a thin polymer layer is needed. However, thin polymer layers could lead to very low absorption efficiency since the penetration length of incident light for the polymer is typically over 100 nm. For boosting the efficiency of HSCs, typically, inorganic nanowires/nanorods are synthesized and infiltrated with the polymers to form a planar solar cell.[3,4] Since the interdistance of nanowires/nanorods and the thickness of polymer layers are much larger than the diffusion length of the excitons in polymer layers, most of the excitons are not able to reach the interface, giving rise to an energy loss in the case of HSCs with a flat air/solar cell interface.[7,8] This means that polymer layers need to be very thin when considering hole mobilities that are low in conducting polymers (~10^{-4} V cm^{-2} s^{-1}).[9]

From the aforementioned discussion, to better meet the exciton diffusion length in polymers, further optimization of the HSC geometries is still necessary to guarantee efficient light absorption and charge separation since the thickness of the organic layers in HSCs plays an important but opposite role in light absorption and exciton dissociation. That is to say, in terms of the low conversion efficiency, there are currently two major fundamental aspects making HSCs unsuitable for practical applications: (i) inefficient carrier separation, (ii) lack of sufficient light absorption. To aim at (i), different methods to reduce

* Address correspondence to jhhe@cc.ee.ntu.edu.tw.

Received for review July 5, 2011 and accepted October 30, 2011.

Published online October 30, 2011
10.1021/nn202485m

recombination and increase charge separation yield in HSCs were reported employing nanocrystals,[10] carbon nanotubes,[11] core−shell metal oxide nanowires,[12] and interfacial modifiers.[13,14] To aim at (ii), it has been found that the antireflection (AR) coatings of inorganic nanowire arrays (NWAs) exhibit the ability to suppress reflection over a broad range of wavelengths and incident angles, which plays an important role in the performance enhancement of optoelectronic devices.[15−18] The efficient reflection suppression in NWAs is mainly attributed to subwavelength features, which make the nanostructures behave like an effective homogeneous medium with a continuous gradient of refractive index, significantly reducing the reflection through destructive interferences.[19−22] Critical AR features of NWAs, such as broadband, angularly insensitive, and polarization-insensitive characteristics, have been carefully examined.[19−22] Recently, the Si NWA layers using room-temperature galvanic wet etching were found to effectively suppress not only specular but also diffuse reflection.[21,22] The superior AR characteristics demonstrate that NWAs can absorb solar light very efficiently and be potentially applied to PVs.[23−25]

In this study, we demonstrate a strategy employing core−shell NWAs consisting of Si/regioregular poly(3-hexylthiophene) (P3HT) (shown in Figure 1) to eliminate a compromise between light-harvesting and exciton dissociation/charge separation for HSCs. A core−shell geometry that capitalizes on strong light-trapping effect at a variety of wavelengths and angles of incidence (AOIs) increases the amount of photons reaching the radial junction regions due to the smooth transition in refractive index at the air/Si interface, demonstrated by external quantum efficiency (EQE) and spectral, angle-dependent reflectance measurements. The interaction between the incident light and the core−shell NWAs is realized through the simulation based on finite-difference time domain (FDTD) analysis. The P3HT shells with a thickness comparable to the exciton diffusion length display efficient exciton dissociation and charge collection, demonstrated by the internal quantum efficiency (IQE) measurements. Accordingly, Si/P3HT core−shell NWA HSCs exhibit a short-circuit current density (J_{sc}) of 11.69 mA/cm^2 for a η of 0.97%, while the HSCs with thick P3HT layers forming a flat air/P3HT interface showed a J_{sc} of 7.26 mA/cm^2 for a η of 0.74%. Surprisingly, improved crystallinity of P3HT after long-time air mass 1.5 global (AM 1.5G) illumination demonstrated by transmission electron microscopy (TEM) and Raman spectroscopy leads to a giant η improvement of Si/P3HT core−shell NWA HSCs from 0.96% to 2.31%. This is due to the considerable increase in open-circuit voltage (V_{oc}) (from 257 to 346 mV), J_{sc} (from 11.7 to 18.9 mA/cm^2), and FF (from 32.2 to 35.2%), which is not observed in conventional P3HT-infiltrated Si NWA HSCs with flat air/polymer interfaces. The stability of the Si/P3HT core−shell NWA HSCs in air ambient was investigated

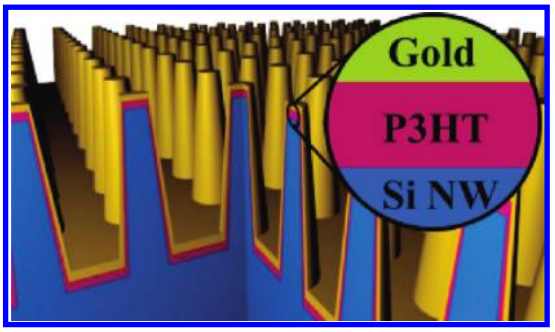

Figure 1. Schematics of Si/P3HT core−shell NWA HSCs.

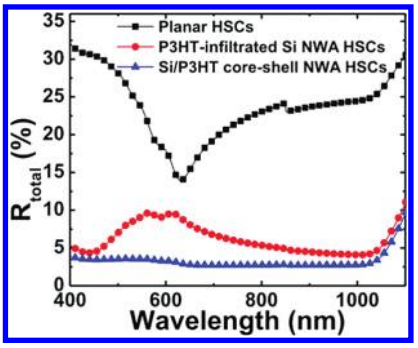

Figure 2. Total reflectance of planar HSCs, P3HT-infiltrated Si NWA HSCs, and Si/P3HT core−shell NWA HSCs.

systematically. The concept of the core−shell NWA geometry reported herein is not limited to Si nanowires and is useful in improving the efficiency or reducing the material consumption for many other solar material systems, opening a new avenue for third-generation solar cells.

RESULTS AND DISCUSSION

In order to emphasize the importance of the core−shell geometry on the light-harvesting performance, total reflectance measurement using an integrating sphere was carried out with three kinds of morphologies of P3HT/Si HSCs, namely, planar HSCs with flat interfaces, P3HT-infiltrated Si NWA HSCs with flat air/polymer interfaces, and Si/P3HT core−shell NWA HSCs, shown in Figure S1 in the Supporting Information. The total reflectance spectra were obtained at the incident angle of 5° and wavelengths ranging from 400 to 1100 nm, as shown in Figure 2. For the planar HSCs with flat P3HT layers on polished Si, the reflectance reaches a minimum at around 620 nm but gradually increases as the wavelength moves toward the UV regions and NIR regions, indicating the behavior of a typical $\lambda/4$ layer. After introducing Si NWAs into HSCs, the reflectance is suppressed over the broadband ranges. Si NWAs embedded in P3HT layers play the role of a graded layer, alleviating the drastic change in the refractive index between air and Si substrates. However, the deposition of thick P3HT layers leads to optically flat interfaces between air and P3HT, still

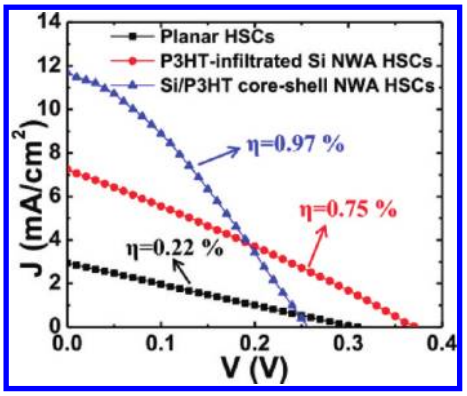

Figure 3. *J*–*V* curves of the three kinds of HSCs under the illumination of an AM 1.5G solar simulator in air ambient measured immediately after the sequential fabrication processes.

yielding unsatisfactory light-trapping ability. The superior light-trapping performances of the core–shell structure are demonstrated in Figure 2 and can be attributed to the additional grading in the effective refractive index profile contributed by thin P3HT shells, which makes the air/Si interfaces less abrupt and therefore facilitates more photons traveling from air to the Si/P3HT NWAs. These results lead us to conclude that the morphologies of the HSCs affect significantly their light-trapping ability.

To estimate the efficiency of converting absorbed photons to collected electrons, current density–voltage (*J*–*V*) curves of the three kinds of HSCs under the illumination of an AM 1.5G solar simulator at 100 mW/cm^2 were measured immediately after the sequential fabrication processes, including formation of Si NWAs, polymer coating, and contact metal deposition, as shown in Figure 3. The photovoltaic characteristics are listed in Table 1. As compared to a η of 0.22% from HSCs with planar Si, HSCs based on P3HT-infiltrated Si NWAs with flat air/P3HT interfaces achieve a η of 0.75%, indicating that the morphology of the heterojunction is important, as such HSC devices with Si NWAs increase interfacial areas. Under AM 1.5G illumination, the P3HT-infiltrated Si NWA HSCs show a J_{sc} of 7.26 mA/cm^2, a V_{oc} of 371 mV, and an FF of 27.5% for a η of 0.75%, while Si/P3HT core–shell NWA HSCs exhibit a J_{sc} of 11.69 mA/cm^2, a V_{oc} of 257 mV, and an FF of 32.2% for a η of 0.97%. A J_{sc} up to 11.69 mA/cm^2 obtained with core–shell NWA HSCs indicates that the geometry of core–shell nanostructured HSCs contributing to more sufficient light absorption offers an advantage over the conventional hybrids with a flat air/P3HT interface using thick P3HT layers. This optical enhancement will be discussed using the simulation and the EQE measurements later. Moreover, Si/P3HT core–shell NWA HSCs with the thickness of P3HT layers comparable to the exciton diffusion length provide efficient charge separations, also contributing to the enhanced J_{sc}.[26] In contrast, for the P3HT-infiltrated NWA HSCs, a flat air/P3HT interface is obtained and

TABLE 1. Device Characteristics of Planar HSCs, P3HT-Infiltrated Si NWA HSCs, and Si/P3HT Core–Shell NWA HSCs

device	J_{sc} (mA/cm^2)	V_{oc} (mV)	FF (%)	η (%)
planar	2.93	309	24.3	0.22
P3HT-ifiltrated Si NWA	7.26	371	27.5	0.74
Si/P3HT core–shell NWA	11.69	257	32.2	0.97

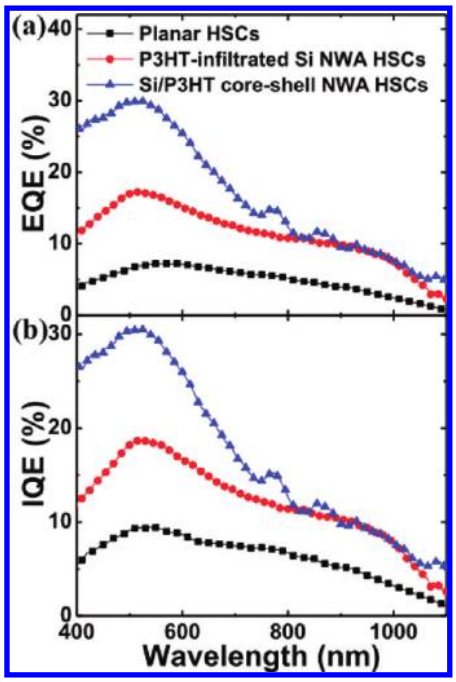

Figure 4. (a) EQE and (b) IQE spectra of planar HSCs, P3HT-infiltrated Si NWA HSCs, and Si/P3HT core–shell NWA HSCs.

the P3HT thickness is much larger than the exciton diffusion length, giving rise to high reflection loss, few excitons successfully diffusing to the junctions, and only a fraction of the dissociated excitons collected by the electrodes. Note that a high reverse saturation current obtained with core–shell HSCs (in Figure S2 in the Supporting Information) produces a reduction in V_{oc}.[27] Increased reverse saturation current is suspectedly due to nonconformal deposition of the metal electrodes over a high aspect-ratio surface of core–shell HSCs.

It is important to gain insight into the correlation between J_{sc} enhancement and optical absorption/carrier collection enhancement in the active layer. The maxima of EQE values of Si/P3HT core–shell NWA and P3HT-infiltrated Si NWA HSCs reach 29.94% and 17.22%, respectively, while 7.22% is achieved for the planar Si-based HSCs, as shown in Figure 4a. A broadband EQE spectrum (400–1100 nm) of the planar Si/P3HT devices shows that a photocurrent is generated by both of P3HT and Si. The enhancement in EQE values after introducing NWA structures implies a pronounced light-trapping ability in subwavelength

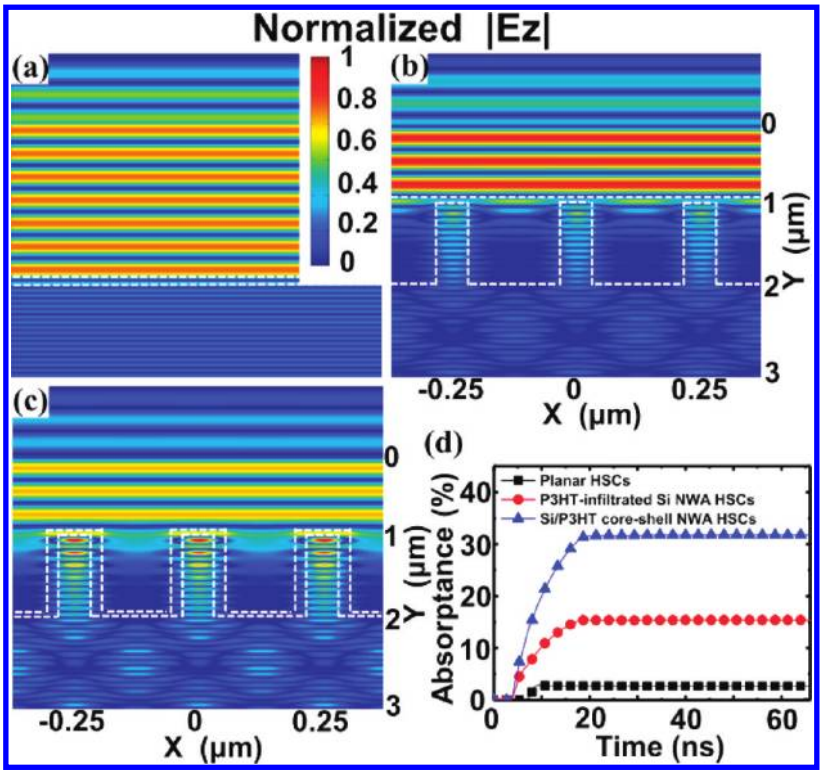

Figure 5. Time-averaged, normalized TE electric field distribution ($|E_z|$) of (a) planar HSCs, (b) P3HT-infiltrated Si NWA HSCs, and (c) Si/P3HT core−shell NWA HSCs simulated by FDTD analysis. (d) Optical absorption integrated over the 15 nm thick P3HT which is near the junction for the three kinds of Si−P3HT morphologies.

nanostructures, which is consistent with the results from reflectance measurements (shown in Figure 2). For understanding light-trapping effects in nanostructured HSCs, the numerical simulations will be applied later. The IQE measurement is useful in HSCs to investigate if excitation of excitons, exciton diffusion/separation, and carrier collection occurring in the active region are effective. Considering the fraction of the actually absorbed photons by the active layers, the EQE can be converted into the IQE, which is the ratio between the measured J_{sc} and the number of absorbed AM 1.5G photons per unit area and time. As shown in Figure 4b, the increase in IQE values after introducing NWA structures indicates the efficiency enhancement of exciton excitation, exciton diffusion/separation, and carrier collection with increased interfacial areas.[28−33] The further improvement in IQE between 400 and 800 nm obtained for Si/P3HT core−shell NWA HSCs mainly results from the enhanced photocurrent derived from P3HT shells. The reason is that the diffusion length of the exciton in P3HT is lower than 15 nm, and only excitons generated in P3HT within 15 nm of the P3HT/Si interface could possibly diffuse to the interface.[23] A significant amount of the excitons in the P3HT shell of Si/P3HT core−shell NWA HSCs could reach the organic/inorganic interface to undergo charge separation because of the thickness of the P3HT shell being comparable to the exciton diffusion length and thereby enhancing the photocurrent. In contrast, for the devices with a continuously thick P3HT film, only part of absorbed light can generate a photocurrent because of the limited exciton diffusion length in P3HT. In short, the core−shell morphology results in the increase in EQE and IQE, showing that not only are more photons absorbed, but these photons are also more efficiently transferred into collected photocarriers. Moreover, the high carrier mobility in Si reduces the difference in IQEs and EQEs between P3HT-infiltrated Si NWA and Si−P3HT core−shell NWA HSCs at IR wavelength ranges.

To verify that the remarkable photocurrent generation is a result of the core−shell geometry, the light propagation within the HSC structures was simulated by FDTD analysis. The grid sizes are $\Delta x \times \Delta y = 0.006 \times 0.001\ \mu m^2$ in the space domain, and the time step for every calculation is 0.01 fs. Boundaries in x and y directions are surrounded by the 0.5 μm perfectly matching layers to absorb the electromagnetic waves. The excitation source, with an infinite width like that of the periodically extended simulated device structure, is placed at 1 μm from the upper boundary of the HSCs. The wavelength for all simulations is selected to be 500 nm, which is at the strongest irradiance region in the solar spectrum. Details of the simulated structures can be found in Figure S3 in the Supporting Information. Figure 5a−c visualize the time-averaged TE-polarized electric field intensity distributions, $|E_z|$, within the three kinds of HSCs with different morphologies

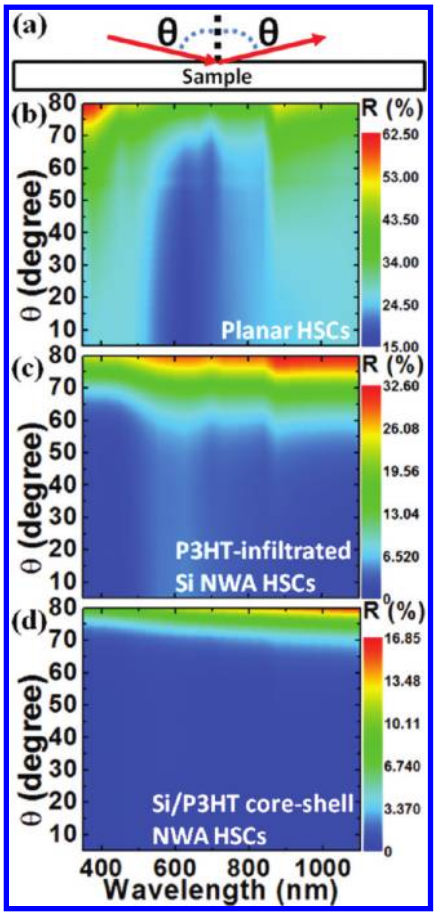

Figure 6. (a) Schematic of AOI-dependent specular reflectance measurement. AOI-dependent specular reflectance spectra on (b) planar HSCs, (c) P3HT-infiltrated Si NWA HSCs, and (d) Si/P3HT core–shell NWA HSCs at AOIs ranging from 5° to 80° and the wavelength range 350–1100 nm.

of Si–P3HT. Details of simulated structures and parameters can be found in Figure S3 in the Supporting Information. All of the calculated values are normalized to the ones of the excitation source. One can see that the NWA structure has a great influence on the light-trapping effect. Similar to the results of the total reflectance measurement, FDTD analysis shows that Si/P3HT core–shell NWA HSCs exhibit excellent optical confinements. For P3HT-infiltrated Si NWA HSCs with thick P3HT layers, a high absorption coefficient of P3HT ($\sim$104 cm^{-1}) causes most of photons to be absorbed at the interface between air and P3HT instead of at the P3HT/Si junctions, leading to insufficient excitons diffusing to the junction successfully and thus inadequate photoexcited carriers collected.[34] For Si/P3HT core–shell NWA HSCs (Figure 5c), the P3HT shell shows an excellent light-harvesting characteristic through not only preventing the incident waves from bouncing back to the free space but also effectively facilitating the light absorption near junction regions, leading to the enhanced photocurrent. Figure 5d shows normalized, integrated optical absorption for the P3HT regions of 15 nm in thickness near the junctions at the wavelength of 500 nm, as we assume that only excitons generated in P3HT within 15 nm of the P3HT/Si interface could reach the interface, where charge separation takes place, and contribute to the photocurrent.[23] The steady-state absorption values for P3HT layers on planar Si, thick P3HT layers on Si NWAs, and P3HT shells on Si NWAs are 2.71%, 15.39%, and 31.76%, respectively. The results indicate that the number of the photons reaching the active region can be drastically increased by introducing a Si/P3HT core–shell structure, further supporting the enhancement of J_{sc} of Si/P3HT core–shell NWA HSCs.

Since the incident sunlight impinges from different directions during a day, a desirable AR coating must eliminate the reflection over wide AOIs efficiently, which is called omnidirectionality. To demonstrate the omnidirectionality of the core–shell geometry of HSCs, the specular reflectance spectra on HSCs with the three kinds of Si–P3HT morphologies was measured at AOIs ranging from 5° to 80°. At every AOI, the incident wavelength was varied in the range 350–1100 nm. The measurement schematic and the results are presented in Figure 6a–d. For the HSCs using planar Si, the reflectance at most wavelengths is noticeably increased for the AOI above 50°, as shown in Figure 6b, indicating that surface reflection cannot be suppressed at high AOIs. It is noted that a slight oscillation of reflectance for HSCs with P3HT film-coated planar Si occurs. This is attributed to the interference between the light reflected at the air/P3HT and the P3HT/Si interfaces, which constitute a Fabry-Pérot microcavity.[35] The high-AOI reflectance is mitigated for the thick P3HT-infiltrated Si NWA HSCs (Figure 6c); the reflectance is effectively reduced for the AOI up to 60°, but only for wavelengths below 850 nm. For Si/P3HT core–shell NWA HSCs (Figure 6d), the AOI limit is further pushed to 75°, below which the reflectance is less than 5% for all the wavelengths. The results in Figure 6b–d clearly demonstrate that the core–shell geometry of HSCs can suppress the undesired Fresnel reflection for not only broadband ranges but also a wide range of AOIs.

Figure 7a shows the illumination time-dependent J–V curves of Si/P3HT core–shell NWA devices under the illumination of an AM 1.5G solar simulator in air ambient, which were obtained immediately after the sequential fabrication processes. We recorded η, V_{oc}, J_{sc}, and FF as a function of AM 1.5G illumination times, as shown in Figure 7b–e, respectively. Si/P3HT core–shell NWA HSCs show a considerable improvement in η from 0.96% to 2.31% after long-time illumination, due to the increase in V_{oc} (from 257 to 346 mV), J_{sc} (from 11.7 to 18.9 mA/cm^2), and FF (from 32.2% to 35.2%). The increase of 34.6% in V_{oc} could be due to the improved crystallinity of P3HT layers during the AM 1.5G illumination, which results in a more efficient charge collection by improving built-in electric

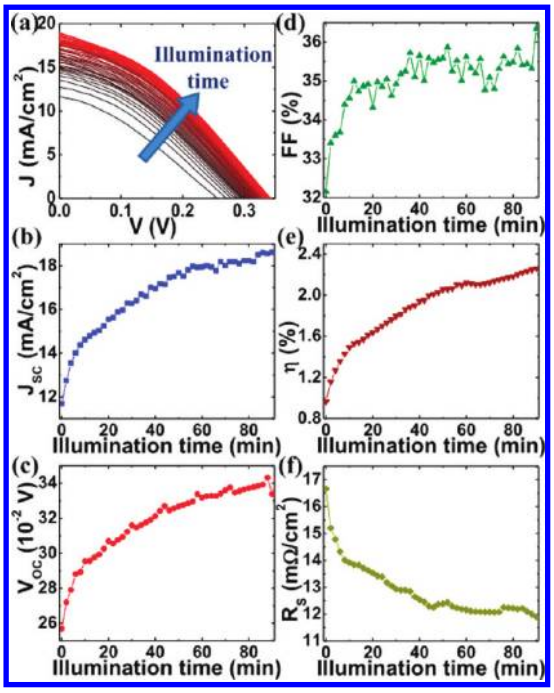

Figure 7. (a) $J-V$ characteristics as a function of the AM 1.5G irradiation time for Si/P3HT core−shell NWA HSCs. (b) V_{oc}, (c) J_{sc}, (d) FF, (e) η, and (f) series resistance (R_s) as a function of the AM 1.5 G illumination time extracted from (a).

fields.[36,37] Improved crystallinity of the P3HT shell layers (*i.e.*, the higher ordering of intrachain interactions in P3HT) will be further confirmed by high-resolution TEM observation and Raman spectroscopy later. Similarly, the improved crystallinity of the P3HT layers during long-time AM 1.5G illumination increases the J_{sc} by 61.5%, suggesting that more charges are extracted from the solar cells due to the improved efficiency in the exciton dissociation and the carrier collection. The efficiency of HSCs is significantly influenced by the mobility of conjugated polymers.[38] Since the hole mobility in conjugated polymers is much lower than the electron mobility in inorganic materials for HSCs, the hole accumulation in the device and thus space-charge effects occur.[31] The hole mobility of conjugated polymers increases when becoming more crystalline.[39] An improved FF value under the illumination suggests an improved balance of electron and hole transport in the HSCs due to increased hole mobility caused by the increased crystallinity degree of the P3HT layers.[31] As shown in Figure 7f, the series resistance of core−shell NWA HSCs measured from the $J-V$ characteristics is reduced from 16.7 to 12.1 mΩ-cm^2 after long-time AM 1.5G illumination, indicating that the efficiency of charge transport and/or collection is improved after 90 min AM 1.5G illumination. This result is consistent with the previous discussion as well because a lower series resistance is expected for a more ordered P3HT film.

As shown in Figure 8, after the 90 min illumination, a significant increase in EQE values in the wavelength

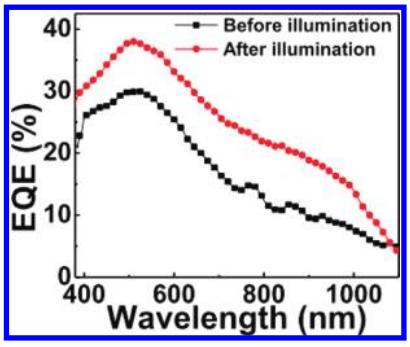

Figure 8. EQE spectra of Si/P3HT core−shell NWA HSCs before and after AM 1.5G illumination for 90 min.

range 400−1100 nm and a slight red-shift of the EQE peak were observed. The increase in EQE values indicates that excitation of excitons, exciton diffusion/separation, and carrier collection are more effective due to improved crystallinity of P3HT shells.[28−33] A slight red-shift of the EQE peak values is also attributed to the improved crystallinity since the better ordering of intrachain interactions in P3HT shells leads to more delocalized conjugated π electrons, reduction of the band gap between π and π^*, and increase of the optical $\pi-\pi^*$ transition.[10] Moreover, the improved crystallinity of P3HT gives rise to enhanced EQE values in NIR regions as well due to the effective collection of photocarriers contributed from Si cores.

The speculation about the improved crystallinity of P3HT after AM 1.5G illumination is further supported by TEM observations and Raman spectroscopy, which provide structural information on the P3HT shells. Figure 9a shows the as-synthesized core−shell nanowire structures with around 25 nm thick P3HT shells before AM 1.5G irradiation. The high-resolution TEM image of the as-synthesized core−shell HSCs (Figure 9b) shows the amorphous nature of the P3HT shells, which can be identified as a culprit for inferior initial photovoltaic characteristics. Figure 9c indicates the presence of a 5 nm thick fringe structure made of oriented crystalline lamellae of P3HT at the interface of Si nanowires after AM 1.5G irradiation for 90 min. The fringes are indicative of a stacked structure with an out-of-plane spacing of the polymer chain layers.[40,41] From a kinetic point of view, it is easier to crystallize at the heterointerface of Si/P3HT as the energy barrier for the nucleation is low, and thus the nucleation rate increases at the heterointerface, which is called heteronucleation. To further support the TEM observation about the reorganization processes of the P3HT layers occurring during AM 1.5G illumination, Raman spectroscopy was utilized to observe the nanoscale change in the P3HT layers by *ex situ* monitoring of the vibrational modes. It has been reported that Raman shifts correspond to the degree of π-electron delocalization along the main chain axis and the interchain interaction.[33,42−44] The characteristics of the −C═C−

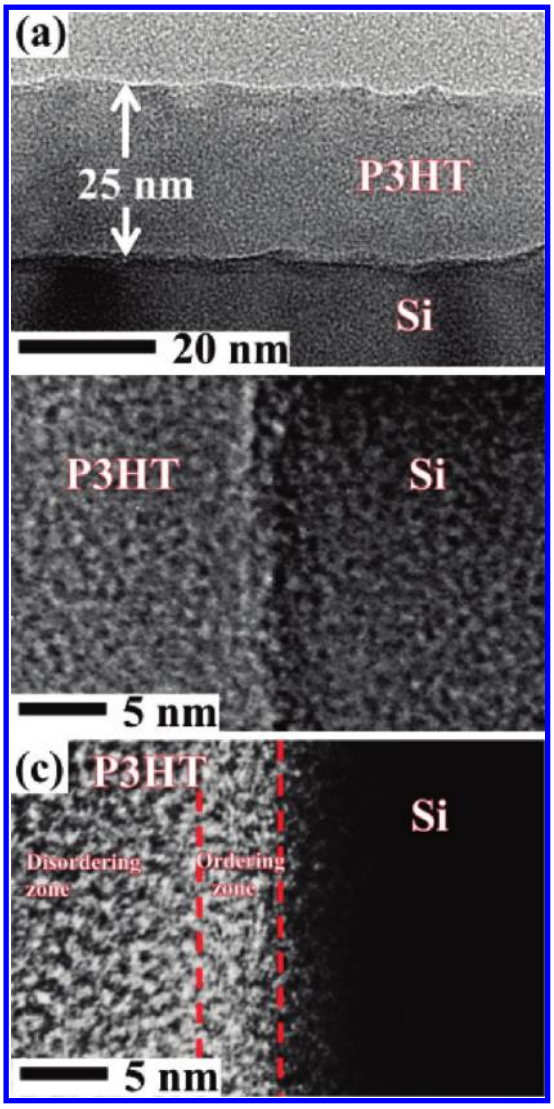

Figure 9. (a) TEM image and (b) high-resolution TEM image of Si/P3HT core−shell NWA HSCS before AM 1.5G illumination for 90 min. (c) High-resolution TEM image of Si/P3HT core−shell NWA HSCs after AM 1.5G illumination for 90 min.

symmetric stretching band ($\nu_{C=C}$) correlate with the changes in the P3HT conformation and the conjugation length. For example, it was found that the increased crystallized size and better internal order within the P3HT domains obtained after annealing result in narrowing and weakening $\nu_{C=C}$.[30,31,45,46] Figure 10a shows the Raman spectra of Si/P3HT core−shell NWAs as a function of the illumination time, indicating the increase in the Raman shift with the illumination time. The peaks at 1440−1445 and 1370−1380 cm^{-1} are ascribed to the −C═C− and the −C−C− skeletal stretching of the thiophene ring, respectively.[10,23,29,43,45] Illumination time-dependent peak area and full width at half-maximum (fwhm) of the $\nu_{C=C}$ Raman band are shown in Figure 10b and c, respectively. The decreases in peak area and fwhm of the $\nu_{C=C}$ from Si/P3HT core−shell NWAs after the long-time illumination correspond to the increased

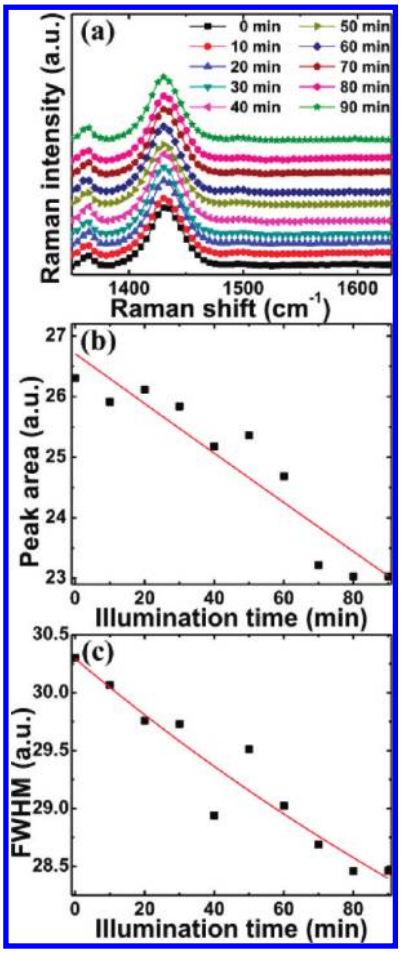

Figure 10. (a) Raman spectra of Si/P3HT core−shell NWA HSCs as a function of illumination time. (b) Peak area and (c) fwhm of a carbon double bond of Si/P3HT core−shell NWA HSCs with the illumination time extracted from (a).

crystallinity within the P3HT layers. The changes in the Raman spectra correlate with the changes in photovoltaic parameters, EQE, and TEM observations of Si/P3HT core−shell NWA HSCs, demonstrating that AM 1.5G illumination indeed leads to substantial ordering in the P3HT shells on Si NWAs. It has been reported that because the internal P3HT ordering is nonoptimal after spin coating, altering the ordering of P3HT by thermal annealing is important for improving the performance of HSCs; the lamella-type stacking of the side chains and the stacking of thiophene rings can affect the absorption, EQE peaks, EQE values, and Raman spectrum of P3HT.[33,37,42−44,47−49] The performance enhancement after the light illumination is an effect of light-induced crystallization, which is similar to annealing-induced crystallization observed in the polymer solar cells with heat treatment.[31,50−52]

To distinguish the importance of improved crystallinity of P3HT shells in the photovoltaic performance of Si/P3HT core−shell NWA HSCs, we compare the illumination time-dependent photovoltaic characteristics of Si/P3HT core−shell NWA HSCs to those of P3HT-infiltrated Si NWA HSCs, as shown in Figure S4 in the

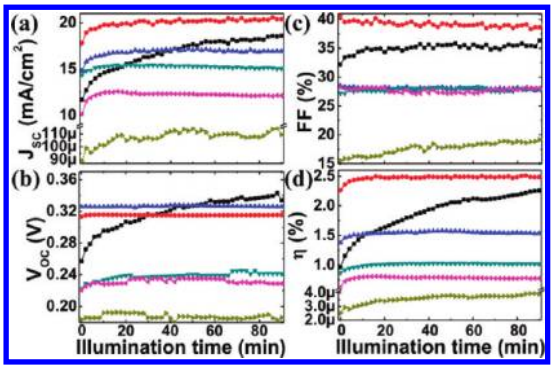

Figure 11. (a) J_{sc}, (b) V_{oc}, (c) FF, and (d) η *versus* irradiation time for as-deposited Si/P3HT core–shell NWA HSCs (■) and those aged in air ambient for 1 (●), 5 (▲), 10 (▼), 15 (▶), and 30 (◀) days.

Supporting Information. Generally, the performance enhancement of P3HT-infiltrated Si NWA HSCs with AM 1.5G illumination is observed as well and is significantly lower than that of Si/P3HT core–shell NWA HSCs. Since the illumination induces the crytallization of 5 nm thick P3HT layers from the Si interface, the ratio of ordering structures of P3HT to entire P3HT layers for Si/P3HT core–shell NWA HSCs is larger than that for P3HT-infiltrated Si NWA HSCs. Accordingly, the improvement of photovoltaic performance is more pronounced in core–shell NWA HSCs with AM 1.5G illumination. For example, J_{sc} climbs rapidly in the core–shell NWA HSCs as compared with that of HSCs containing P3HT-infiltrated Si NWAs, which can be assigned to more efficient carrier collection. This is further confirmed by EQE measurements, as shown in Figure S5 in the Supporting Information. After long-time illumination, the EQE value for P3HT-infiltrated Si NWA HSCs was increased slightly, while that of Si/P3HT core–shell NWA HSCs was increased significantly. This is because the thick P3HT thwarts the exciton dissociation and the hole transfer/collection by electrodes.[31]

For practical applications, the stability of the polymer-based photovoltaic device in air ambient is an important issue. We stored the Si/P3HT core–shell NWA HSCs in air ambient in the dark after every illumination time-dependent measurement to evaluate their long-term stability without encapsulation. Figure 11 shows the decline of the photovoltaic characteristics, J_{sc}, V_{oc}, FF, and η, with storing times. Storing the Si/P3HT core–shell NWA HSCs in air ambient in the dark after the illumination time-dependent measurements did not cause significant degradation of device performances for the first day. Unprotected core–shell NWA HSCs degraded significantly for over 1 day, but did not become completely trivial and still exhibited improved photovoltaic characteristics upon AM 1.5G illumination even after 30 days of continuous exposure to air; although P3HT degradation in air ambient was observed, the P3HT self-organization upon illumination also could be observed. It has been known that O_2 and H_2O are responsible for the polymer degradation observed for the devices under ambient conditions.[53,54]

CONCLUSION

With Si/P3HT core–shell NWA morphology using easily accessible chemical etching and spin-coating techniques, surface reflection and charge recombination are substantially inhibited in HSCs. Core–shell NWA HSCs with thin P3HT layers that are fitted with effective light-trapping Si NWA systems can therefore achieve the absorption equivalent to the HSCs with a much thicker P3HT layer and still retain their efficient exciton separation/carrier collection properties, resulting in enhanced EQE and IQE for a η improvement of 31.1% as compared to the P3HT-infiltrated NWA HSCs forming a flat air/solar cell interface. The effect of AM 1.5G illumination on core–shell NWA HSC performance has been investigated. It was found that for core–shell NWA HSCs even very thin illumination-induced P3HT ordering (~5 nm in thickness) at the junction leads to a giant improvement in V_{oc} from 257 to 346 mV, J_{sc} from 11.7 to 18.9 mA/cm^2, and FF from 32.2% to 35.2% with η from 0.96% to 2.31%. Although the ideal donor–acceptor morphology for HSCs is unknown, there are hints that core–shell nanostructures provide efficient light-harvesting medium and come close to the optimum in terms of excitation of excitons, exciton diffusion/separation, and carrier collection. The present study offers a novel direction for high-efficiency and low-cost HSCs by introducing the core–shell geometry.

EXPERIMENTAL SECTION

Single-crystalline n-type Si(001) substrates, 550 μm thick, with ρ = 1–10 Ω-cm were used to fabricate NWAs. The substrates were first cleaned in acetone, followed by a HF dip to remove the native oxide from the surfaces. The cleaned Si substrates were then immersed into an aqueous HF solution containing 0.03 mol/L silver nitrate at 25 °C for 30 min. The concentration of HF for all the samples was 4.6 M. Residual aggregated silver particles formed on the Si NWAs could be removed by immersing into nitric acid, and the substrates were cleaned with acetone, 2-propanol, and distilled water. Subsequently the substrates were dried by N_2 gas and treated with O_2 plasma [SAMCO UV Dry-Cleaner (model UV-1)] for 10 min to obtain hydrophilic surfaces for spin coating P3HT uniformly. The fabricated Si NWAs were used for the fabrication of 3D heterojunction hybrid solar cells with P3HT. Before spin-coating P3HT, bottom ohmic electrodes were deposited by electron-gun evaporation at a deposition rate of less than 0.1 nm/s with a

chamber pressure of 2×10^{-6} Torr. P3HT was dissolved in chlorobenzene with a concentration of 15 mg/mL. The P3HT solutions were spin-coated over vertically aligned Si NWAs with different spin-speeds in order to form different thicknesses of P3HT layers and dried in air ambient. Finally, we deposited the semitransparent 20 nm thick gold electrodes by electron-gun evaporation to complete our device structures.

A morphological study was performed with JEOL JSM-6500 field emission SEM. Optical measurements were carried out by a standard UV−visible−NIR spectrometer (JASCO ARN-733) with an integrating sphere with a noise level of 0.002%. During the measurements, the wavelength was varied from 380 to 1100 nm. The *J*−*V* curves of the solar cells were measured with a Keithley 4200 source meter under the illumination of an AM 1.5G solar simulator (100 mW/cm^2). The EQEs of the HSCs at the wavelength range 400−1100 nm were measured by coupling a halogen lamp to a monochromator. The Raman spectrum was measured with a Jobin Yvon T64000 triple spectrometer equipped with charged-coupled devices cooled at 160 K. The substrate-bound core−shell NWAs were mechanically scrapped and deposited on carbon-coated copper grids for TEM characterization with a JEOL 3000F TEM.

Acknowledgment. The research was supported by the National Science Council with Grant Nos. 99-2120-M-007-012 and 99-2622-E-002-019-CC3.

Supporting Information Available: Figures S1 to S5. This information is available free of charge via the Internet at http://pubs.acs.org.

REFERENCES AND NOTES

1. Günes, S.; Neugebauer, H.; Sariciftci, N. S. Conjugated Polymer-Based Organic Solar Cells. *Chem. Rev.* **2007**, *107*, 1324–1338.
2. Huynh, W. U.; Dittmer, J. J.; Alivisatos, A. P. Hybrid Nanorod-Polymer Solar Cells. *Science* **2002**, *295*, 2425–2427.
3. Bouclé, J.; Ravirajan, P.; Nelson, J. Hybrid Polymer−Metal Oxide Thin Films for Photovoltaic Applications. *J. Mater. Chem.* **2007**, *17*, 3141–3153.
4. Weickert, J.; Dunbar, R. B.; Hesse, H. C.; Wiedemann, W.; Schmidt-Mende, L. Nanostructured Organic and Hybrid Solar Cells. *Adv. Mater.* **2011**, *23*, 1810–1828.
5. Crossland, E. J. W.; Kamperman, M.; Nedelcu, M.; Ducati, C.; Wiesner, U.; Smilgies, D. M.; Toombes, G. E. S.; Hillmyer, M. A.; Ludwigs, S.; Steiner, U.; *et al*. A Bicontinuous Double Gyroid Hybrid Solar Cell. *Nano Lett.* **2009**, *9*, 2807–2812.
6. Gowrishankar, V.; Scully, S. R.; McGehee, M. D. Exciton Splitting and Carrier Transport Across the Amorphous-Silicon/Polymer Solar Cell Interface. *Appl. Phys. Lett.* **2006**, *89*, 252102-1–252102-3.
7. Halls, J. J. M.; Pichler, K.; Friend, R. H.; Moratti, S. C.; Holmes, A. B. Exciton Diffusion and Dissociation in A Poly(p-phenylenevinylene)/C60 Heterojunction Photovoltaic Cell. *Appl. Phys. Lett.* **1996**, *68*, 3120–3122.
8. Grozema, F. C.; Siebbeles, L. D. A.; Gelinck, G. H.; Warman, J. M. The Opto-Electronic Properties of Isolated Phenylenevinylene Molecular Wires. *Top. Curr. Chem.* **2005**, *257*, 135–164.
9. Bozano, L.; Carte, S. A.; Scott, J. C.; Malliaras, G. G.; Brock, P. J. Temperature- and Field-Dependent Electron and Hole Mobilities in Polymer Light-Emitting Diodes. *Appl. Phys. Lett.* **1999**, *74*, 1132–1134.
10. Yildiz, H. B.; Tel-Vered, R.; Willner, I. Solar Cells with Enhanced Photocurrent Efficiencies Using Oligoaniline-Crosslinked Au/CdS Nanoparticles Arrays on Electrodes. *Adv. Funct. Mater.* **2008**, *18*, 3497–3505.
11. Somani1, P. R.; Somani, S. P.; Flahaut, E.; Umeno, M. Improving the Photovoltaic Response of a Poly(3-octylthiophene)/n-Si Heterojunction by Incorporating Double-Walled Carbon Nanotubes. *Nanotechnology* **2007**, *18*, 185708-1–185708-5.
12. Greene, L. E.; Law, M.; Yuhas, B. D.; Yang, P. ZnO-TiO_2 Core-Shell Nanorod.P3HT Solar Cells. *J. Phys. Chem. C* **2007**, *111*, 18451–18456.
13. Lin, Y. Y.; Lee, Y. Y.; Chang, L.; Wu, J. J.; Chen, C. W. The Influence of Interface Modifier on the Performance of Nanostructured ZnO/Polymer Hybrid Solar Cells. *Appl. Phys. Lett.* **2009**, *94*, 063308-1–063308-3.
14. Goh, C.; Scully, S. R.; McGehee, M. D. Effects of Molecular Interface Modification in Hybrid Organic-Inorganic Photovoltaic Cells. *J. Appl. Phys.* **2007**, *101*, 114503-1–114503-12.
15. Tsai, D. S.; Lin, C. A.; Lien, W. C.; Chang, H. C.; Wang, Y. L.; He, J. H. Ultrahigh Responsivity Broadband Detection of Si Metal-Semiconductor-Metal Schottky Photodetectors Improved by ZnO Nanorod Arrays. *ACS Nano* **2011**, *5*, 7748–7753.
16. Yeh, L. K.; Lai, K. Y.; Lin, G. J.; Fu, P. H.; Chang, H. C.; Lin, C. A.; He, J. H. Giant Efficiency Enhancement of GaAs Solar Cells with Graded Antireflection Layers Based on Syringelike ZnO Nanorod Arrays. *Adv. Energy Mater.* **2011**, *1*, 506–510.
17. Fan, Z.; Kapadia, R.; Leu, P. W.; Zhang, X.; Chueh, Y. L.; Takei, K.; Yu, K.; Jamshidi, A.; Rathore, A. A.; Ruebusch, D. J.; *et al*. Ordered Arrays of Dual-Diameter Nanopillars for Maximized Optical Absorption. *Nano Lett.* **2010**, *10*, 3823–3827.
18. Lien, W. C.; Tsai, D. S.; Chiu, S. H.; Senesky, D. G.; Maboudian, R.; Pisano, A. P.; He, J. H. Low-Temperature, Ion Beam Assisted SiC Thin Films with Antireflective ZnO Nanorod Arrays for High-Temperature Photodetection. *IEEE Electron Device Lett.* **2011**, *32*, 1564–1566.
19. Chao, Y. C.; Chen, C. Y.; Lin, C. A.; Dai, Y. A.; He, J. H. Antireflection Effect of ZnO Nanorod Arrays. *J. Mater. Chem.* **2010**, *20*, 8134–8138.
20. Chao, Y. C.; Chen, C. Y.; Lin, C. A.; He, J. H. Light Scattering by Nanostructured Anti-Reflection Coatings. *Energy Environ. Sci.* **2011**, *4*, 3436–3441.
21. Chang, H. C.; Lai, K. U.; Dai, Y. A.; Wang, H. H.; Lin, C. A.; He, J. H. Nanowire Arrays with Controlled Structure Profiles for Maximizing Optical Collection Efficiency. *Energy Environ. Sci.* **2011**, *4*, 2863–2869.
22. Dai, Y. A; Chang, H. C.; Lai, K. Y.; Lin, C. A.; Chung, R. J.; Lin, G. R.; He, J. H. Subwavelength Si Nanowire Arrays for Self-Cleaning Antireflection Coatings. *J. Mater. Chem.* **2010**, *20*, 10924–10930.
23. Garnett, E. C.; Yang, P. Silicon Nanowire Radial p-n Junction Solar Cells. *J. Am. Chem. Soc.* **2008**, *130*, 9224–9225.
24. Sivakov, V.; Andrä, G.; Gawlik, A.; Berger, A.; Plentz, J.; Falk, F.; Christiansen, S. H. Silicon Nanowire-Based Solar Cells on Glass: Synthesis, Optical Properties, and Cell Parameters. *Nano Lett.* **2009**, *9*, 1549–1554.
25. Stelzner, T.; Pietsch, M.; Andra1, G.; Falk, F.; Ose1, E.; Christiansen, S. Silicon Nanowire-Based Solar Cells. *Nanotechnology* **2008**, *19*, 295203-1–295203-4.
26. Li, G.; Shrotriya, V.; Yao, Y.; Yang, Y. Investigation of Annealing Effects and Film Thickness Dependence of Polymer Solar Cells Based on Poly(3-hexylthiophene). *J. Appl. Phys.* **2005**, *98*, 043704-1–043704-5.
27. Lloyd, M. T.; Lee, Y. J.; Davis, R. J.; Fang, E.; Fleming, R. M.; Hsu, J. W. P.; Kline, R. J.; Toney, M. F. Improved Efficiency in Poly(3-hexylthiophene)/Zinc Oxide Solar Cells via Lithium Incorporation. *J. Phys. Chem. C* **2009**, *113*, 17608–17612.
28. Hoppea, H.; Sariciftci, N. S. Organic Solar Cells: An Overview. *J. Mater. Res.* **2004**, *19*, 1924–1945.
29. Gunes, S.; Sariciftci, N. S. Hybrid Solar Cells. *Inorg. Chim. Acta* **2008**, *361*, 581–588.
30. Olson, D. C.; Shaheen, S. E.; Collins, R. T.; Ginley, D. S. The Effect of Atmosphere and ZnO Morphology on the Performance of Hybrid Poly(3-hexylthiophene)/ZnO Nanofiber Photovoltaic Devices. *J. Phys. Chem. C* **2007**, *111*, 16670–16678.
31. Li, G.; Shrotriya, V.; Huang, J.; Yao, Y.; Moriarty, T.; Emery, K. High-Efficiency Solution Processable Polymer Photovoltaic Cells by Self-Organization of Polymer Blends. *Nat. Mater.* **2005**, *4*, 864–868.
32. Gonzalez-Valls, I.; Lira-Cantu, M. Vertically-Aligned Nanostructures of ZnO for Excitonic Solar Cells: A Review. *Energy Environ. Sci.* **2009**, *2*, 19–34.
33. Miller, S.; Fanchini, G.; Lin, Y. Y.; Li, C.; Chen, C. W.; Su, W. F.; Chhowalla, M. Investigation of Nanoscale Morphological

Changes in Organic Photovoltaics during Solvent Vapor Annealing. *J. Mater. Chem.* **2008**, *18*, 306–312.
34. Zhokhavets, U.; Erb, T.; Gobsch, G.; Al-Ibrahim, M.; Ambacher, O. Relation Between Absorption and Crystallinity of Poly(3-hexylthiophene)/Fullerene Films for Plastic Solar Cells. *Chem. Phys. Lett.* **2006**, *418*, 347–350.
35. Chen, H. Y.; Lin, H. W.; Wu, C. Y.; Chen, W. C.; Chen, J. S.; Gwo, S. Gallium Nitride Nanorod Arrays as Low-Refractive-Index Transparent Media in the Entire Visible Spectral Region. *Opt. Express* **2008**, *16*, 8106–8116.
36. Jiang, X.; Dai, J.; Wang, H.; Geng, Y.; Yan, D. Organic Photovoltaic Cells Using Hexadecafluorophthalocyaninatocopper (F_{16}CuPc) as Electron Acceptor Material. *Chem. Phys. Lett.* **2007**, *446*, 329–332.
37. Bavel, S. S.; van; Bärenklau, M.; With, G.; de; Hoppe, H.; Loos, J. P3HT/PCBM Bulk Heterojunction Solar Cells: Impact of Blend Composition and 3D Morphology on Device Performance. *Adv. Funct. Mater.* **2010**, *20*, 1458–1463.
38. Dittmer, J. J.; Marseglia, E. A.; Friend, R. H. Electron Trapping in Dye/Polymer Blend Photovoltaic Cells. *Adv. Mater.* **2000**, *12*, 1270–1274.
39. Casado, J.; Hicks, R. G.; Hernández, V.; Myles, D. J. T.; Ruiz Delgado, M. C.; López Navarrete, J. T. Infrared and Raman Features of A Series of α,ω-bis(arylthio)oligothiophenes as Molecular Wires. A π-electron Delocalization Efficiency Study. *J. Chem. Phys.* **2003**, *118*, 1912–1920.
40. Briseno, A. L.; Holcombe, T. W.; Boukai, A. I.; Garnett, E. C.; Shelton, S. W.; Fréchet, J. J. M.; Yang, P. Oligo- and Polythiophene/ZnO Hybrid Nanowire Solar Cells. *Nano Lett.* **2010**, *10*, 334–340.
41. Brinkmann, M.; Wittmann, J. C. Orientation of Regioregular Poly(3-hexylthiophene) by Directional Solidification: A Simple Method to Reveal the Semicrystalline Structure of a Conjugated Polymer. *Adv. Mater.* **2006**, *18*, 860–863.
42. Yun, J. J.; Peet, J.; Cho, N. S.; Bazan, G. C.; Lee, S. J.; Moskovits, M. Insight into the Raman Shifts and Optical Absorption Changes upon Annealing Polymer/Fullerene Solar Cells. *Appl. Phys. Lett.* **2008**, *92*, 251912-1–251912-3.
43. Klimov, E.; Li, W.; Yang, X.; Hoffmann, G G.; Loos, J. Scanning Near-Field and Confocal Raman Microscopic Investigation of P3HT-PCBM Systems for Solar Cell Applications. *Macromolecules* **2006**, *39*, 4493–4496.
44. Huang, Y. C.; Liao, Y. C.; Li, S. S.; Wu, M. C.; Chen, C. W.; Su, W. F. Study of the Effect of Annealing Process on the Performance of P3HT/PCBM Photovoltaic Devices Using Scanning-Probe Microscopy. *Sol. Energy Mater. Sol. Cells* **2009**, *93*, 888–892.
45. Ravirajan, P.; Haque, R. A.; Durrant, J. R; Bradley, D. D. C.; Nelson, J. The Effect of Polymer Optoelectronic Properties on the Performance of Multilayer Hybrid Polymer/TiO_2 Solar Cells. *Adv. Funct. Mater.* **2005**, *15*, 609–618.
46. Arnautov, S. A.; Nechvolodova, E. M.; Bakulinb, A. A.; Elizarov, S. G.; Khodarev, A. N.; Martyanov, D. S.; Paraschuk, D. Y. Properties of MEH-PPV Films Prepared by Slow Solvent Evaporation. *Synth. Met.* **2004**, *147*, 287–291.
47. Kim, H.; So, W. W.; Moon, S. J. Effect of Thermal Annealing on the Performance ofP3HT/PCBM Polymer Photovoltaic Cells. *J. Korean Phys. Soc.* **2006**, *48*, 441–445.
48. Ko, C. J.; Lin, Y. K.; Chen, F. C. Microwave Annealing of Polymer Photovoltaic Devices. *Adv. Mater.* **2007**, *19*, 3520–3523.
49. Koster, L. J. A.; Mihailetchi, V. D.; Blom, P. W. M. Ultimate Efficiency of Polymer/Fullerene Bulk Heterojunction Solar Cells. *Appl. Phys. Lett.* **2006**, *88*, 093511-1–093511-3.
50. Kim, D. H.; Jang, Y.; Park, Y. D.; Cho, K. Surface-Induced Conformational Changes in Poly(3-hexylthiophene) Monolayer Films. *Langmuir* **2005**, *21*, 3203–3206.
51. Campoy-Quiles, M.; Ferenczi, T.; Agostinelli, T.; Etchegoin, P. G.; Kim, Y.; Anthopoulos, T. D.; Stavrinou, P. N.; Bradley, D. D. C.; Nelson, J. Morphology Evolution via Self-Organization and Lateral and Vertical Diffusion in Polymer:Fullerene Solar Cell Blends. *Nat. Mater.* **2008**, *7*, 158–164.
52. Kline, R. J.; McGehee, M. D.; Toney, M. F. Highly Oriented Crystals at the Buried Interface in Polythiophene Thin-Film Transistors. *Nat. Mater.* **2006**, *5*, 222–228.
53. Ong, B.; Wu, Y.; Jiang, L.; Liu, P.; Murti, K. Polythiophene-Based Field-Effect Transistors with Enhanced Air Stability. *Synth. Met.* **2004**, *142*, 49–52.
54. Neugebauer, H.; Brabec, C.; Hummelen, J. C.; Sariciftci, N. S. Stability and Photodegradation Mechanisms of Conjugated Polymer/Fullerene Plastic Solar Cells. *Sol. Energy Mater. Sol. Cells* **2000**, *61*, 35–42.